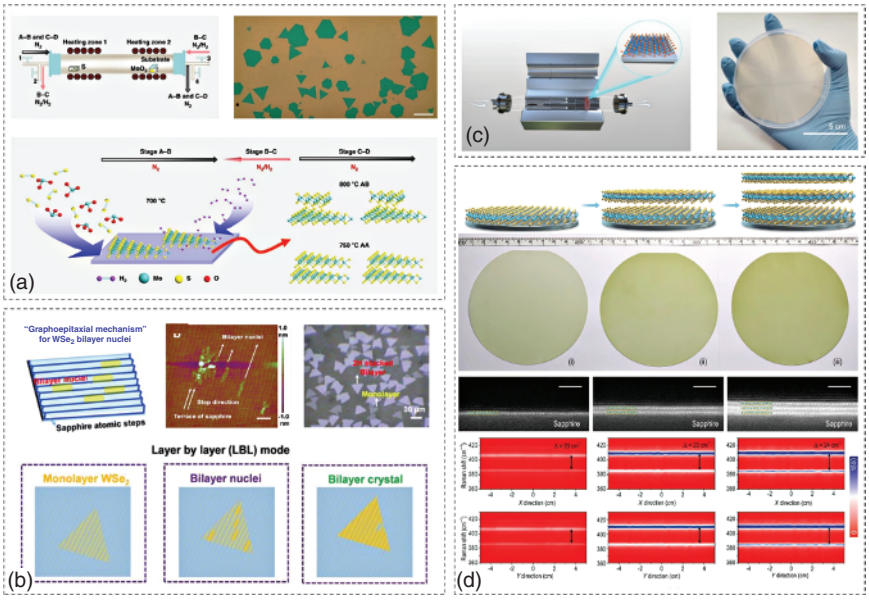

Figure 1.5 Thickness control for CVD growth of 2D materials. (a) Schematic diagram of reverse-flow CVD process for growing bilayer MoS_2 and corresponding OM image of obtained bilayer MoS_2. Source: Xiumei Zhang [71]/Springer Nature/CC BY 4.0. (b) Schematic diagram of the bilayer WSe_2 epitaxy growth process on c-plane sapphire and the corresponding AFM and OM images. Source: Reproduced with permission from Ali Han et al. [72]/Reproduced with permission from Royal Society of Chemistry. (c) Diagram of the CVD growth of wafer-scale (4-inch) $MoSe_2$ in three-temperature-zone tube furnace. Source: Jiawei Li et al. [73]/John Wiley & Sons/CC BY 4.0. (d) Schematic diagram of layer-by-layer epitaxy of multilayer wafer MoS_2 and corresponding photographs, STEM images (cross-section), and Raman spectra line mapping images of the wafers. Source: Qinqin Wang et al. [74]/Oxford University Press/CC BY 4.0.

difficult [70]. Ostrikov et al. developed a reverse-flow CVD growth strategy to prepare the uniform bilayer MoS_2 [71]. The detailed growth produced is shown in Figure 1.5a. Different from the traditional CVD method with constant gas flow direction during the entire growth process, here they introduced a reverse airflow in the variable temperature section (b–c section). This reverse gas flow reduces uncontrolled nucleation and promotes uniform epitaxy of the second monolayer from the active nucleation center on the first monolayer. This approach enables high-quality, uniform bilayer MoS_2 crystals with high yield, controllability, and reliability, and it provides a possible route for the subsequent large-scale growth of 2D materials with controllable layers. Wu et al. successfully grew a controllable three-layer MoS_2 with high mobility and large single crystals on a sodium-lime glass substrate by using a CVD strategy [75]. In addition, Zhang et al. used a similar reverse-flow CVD growth strategy to inhibit the uncontrolled nucleation and thus achieved the highly robust epitaxial growth of various 2D heterogeneous structures and superlattices [51]. Li et al. reported the controlled growth of 2H-stacked bilayer

WSe_2 by CVD growth on a c-plane sapphire substrate with atomic steps, as shown in Figure 1.5b [72]. They demonstrate that the nuclei growth of bilayer WSe_2 slides along the pronounced atomic steps induced by WSe_2 crystals atop, resembling the graphoepitaxy mechanism.

Though great progress has been made in the growth of multilayer TMD grains, achieving wafer-scale multilayer TMD films remains a big challenge. Wang et al. report the step-induced uniform nucleation (>99%) of bilayer MoS_2 on c-plane sapphire [76]. According to DFT calculations, a bilayer nucleation with aligned edges is required before merging to obtain a uniform bilayer TMDs film, and the interfacial formation energy of bilayer MoS_2 markedly decreases with step height. In an experiment, they explored the atomic terrace height on c-plane sapphire to enable an edge-nucleation mechanism and the coalescence of MoS_2 domains into continuous, centimeter-scale films. Moreover, Zhang's group devotes a great effect on the growth of wafer-scale multilayer 2D TMDs. They firstly developed a multi-channel source-supply CVD strategy to grow wafer-scale (4-inch) single-layer $MoSe_2$ film in a three-temperature zone tubular furnace [73]. In this work, they placed the sources in different temperature zones, with the sapphire substrate placed vertically in the third temperature zone. Especially, three small quartz tubes in the growth chamber act as containers for MoO_3, each capable of independently transporting carrier gas. This multi-channel design provides an even and continuous precursor supply, allowing uniform nucleation of $MoSe_2$ across the entire wafer with high nucleation density and the ability to grow wafer-scale monolayers in a short period of time. This work provides an important foundation for the subsequent wafer-scale growth of multilayer TMD films. Zhang et al. report the layer-by-layer epitaxy process growth method for preparing high-quality 4-inch multilayer MoS_2 wafers on sapphire substrate [74]. Firstly, monolayer MoS_2 is prepared by domain-domain coalescence in a multi-channel oxygen-enhanced CVD system. Then, additional epitaxial layers are grown on top of the first layer using the same technique to control the number of layers, resulting in multilayers of MoS_2 with clean, sharp interface atoms. The layer-by-layer epitaxial growth process enables a well-defined stack sequence with precise control over the number of layers, up to six. Furthermore, recent studies have demonstrated the successful synthesis of high-quality wafer-scale multilayer 2D films such as graphene and h-BN by reasonably designing the CVD growth conditions and processes [77–79]. Above progresses on thickness-controllable preparation of 2D materials provides the material foundation for exploring their thickness-dependent properties and device applications. With the development of new CVD technology, it is believed that the thickness-controllable preparation of many other 2D materials will be realized in the near future.

1.6 Phase Control in CVD Growth of 2D Materials

The phase multiplicity of 2D materials is pivotal for exploring their novel physical and chemical properties [80]. For example, most 2D TMDs (MoS_2, WS_2, WSe_2, etc.)

possess a stable 2H phase and a metastable 1T and 1T′ phase, which exhibit semiconducting and metallic properties, respectively [5]. Moreover, researchers found that the semiconducting 2H $MoTe_2$ might be commendable in thermoelectricity [81], and the metallic 1T′ $MoTe_2$ has extremely large magnetoresistance and quantum spin Hall effect [82, 83]. Interestingly, the hexagonal and tetragonal FeTe nanosheets were demonstrated to possess ferromagnetism and antiferromagnetism, respectively [84].

Phase engineering of 2D materials during the CVD growth process is much important to explore their various properties and device applications. One of the important approaches for phase engineering is to realize the phase transformation of existing 2D materials in a CVD system. Ye et al. reported a route for synthesizing wafer-scale single-crystalline 2H $MoTe_2$ by in-plane epitaxial tellurizing, which was triggered by a deliberately implanted single seed crystal [65]. Hu et al. realized a large-scale selective growth of the 1T′/2H/1T′ $MoTe_2$ multiphase structure, with the 1T′ and 2H phases seamlessly stitched [85]. The various phase transformation methods not only provide convenient and effective approaches readily applicable in many applications but also play critical roles in understanding the fundamentals of how crystal phases impact their properties.

Compared with the phase transformation method, the direct synthesis of 2D materials with distinct phase structures is more favorable to achieve a high-purity phase structure. CVD growth has great potential in the phase-controllable synthesis of 2D materials because of its diverse growth parameters (temperature, precursor, carrier gas, composition, etc.) [86]. For example, Jiao et al. reported the phase-selective growth of 1T′ and 2H MoS_2 monolayers and 1T′/2H heterophase bilayers using a potassium (K)-assisted CVD method [87]. This was realized by using K_2MoS_4 as a precursor and tuning the concentration of K in the growth products to invert the stability of the 1T′ and 2H phases. In Figure 1.6a, Xu et al. developed a facile CVD method to synthesize high-quality $Mo_xRe_{1-x}S_2$ alloys with tunable composition and phase structure [88]. The 1T′ phase $Mo_xRe_{1-x}S_2$ alloys were obtained for x in the range of 0–0.25, while the 2H phase $Mo_xRe_{1-x}S_2$ alloys were achieved for x in the range of 0.75–1. Liu et al. selectively synthesized the hexagonal phase and the tetragonal phase FeTe nanosheets on SiO_2/Si by controlling the growth temperature during the CVD process (Figure 1.6b) [84]. The phase-controllable growth of FeTe originates from the formation energy difference between the hexagonal and tetragonal phases, and maintaining a relatively high temperature is essential for obtaining the thermodynamically stable hexagonal phase, while a low temperature is favorable to the tetragonal phase. Most recently, Zhao et al. synthesized both pure β and β′ In_2Se_3 by means of controlling whether to add InSe into the In_2O_3 precursor [89]. Using DFT calculations and in situ TEM experiments, they confirm that the Se deficiency triggers the $\beta \rightarrow \beta'$ phase transition, which effectively explains the seeding effect of InSe additive in CVD precursors for the β′-phase growth. The above results demonstrate the feasibility of CVD synthesis of large-area, highly crystalline 2D materials with controllable phase structures, which is highly desirable for their promising wide applications.

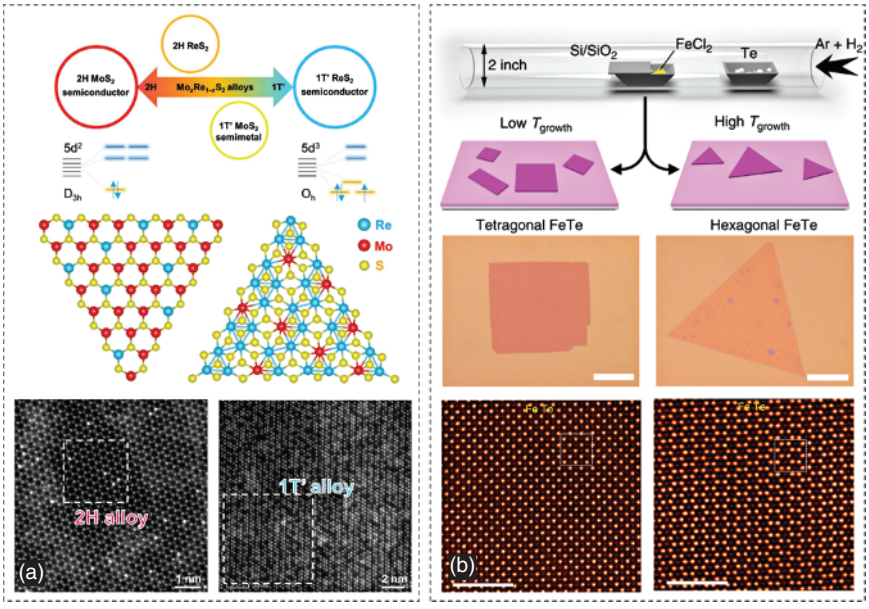

Figure 1.6 Phase-tunable synthesis of 2D materials. (a) Schematic illustration of the structure, phase, and energy band engineering of $Mo_xRe_{1-x}S_2$ alloys, the atomic structure of 2H and 1T′ $Mo_xRe_{1-x}S_2$ alloys, and the ADF-STEM images of 1T′ and 2H $Mo_xRe_{1-x}S_2$ alloys. Source: Reproduced with permission from Qixin Deng et al. [88]/John Wiley & Sons. (b) Schematic view for the temperature-modulated phase selective growth process of FeTe, the OM images (scale bar: 20 μm) and atomic-resolution STEM-ADF images (scale bar: 5 nm) of tetragonal and hexagonal FeTe nanosheets. Source: Lixing Kang et al. [84]/Springer Nature/CC BY 4.0.

1.7 Summary and Prospect

Over the past two decades, the preparation of 2D materials has made tremendous progress, which greatly promotes the fast development of the 2D field. To realize the high-efficiency synthesis of 2D materials with controllable thickness, domain size, crystal quality, and phase structures, researchers have developed a series of preparation approaches, including mechanical exfoliation, LPE, and CVD. The various preparation methods possess their own advantages and disadvantages, and thus the obtained 2D materials exhibit distinct features that fulfill the requirements of their diverse applications. In brief, the mechanical cleavage method can prepare most of the target 2D materials with high crystal quality, but the samples acquired via this approach also possess several problems, such as irregular morphology, uncontrollable thickness, small domain size, and low yield. The corresponding 2D materials are primarily used to explore their fundamental properties. LPE is suitable for large-scale production at a low cost, but precise control of size and layer number with preservation of pristine quality is still highly challenging. The obtained 2D materials exhibit prominent superiorities in some special applications, such as lithium-ion batteries, catalysis, printer ink, and composite materials. Bottom-up

synthesis via CVD growth has emerged as a versatile and scalable approach enabling precise control over the thickness, morphology, crystallinity, and phase structure, which provides significant opportunities for exploring their fundamental physics and device applications.

References

1 Akinwande, D., Huyghebaert, C., Wang, C.-H. et al. (2019). Graphene and two-dimensional materials for silicon technology. *Nature* 573 (7775): 507–518.

2 Giri, A., Park, G., and Jeong, U. (2023). Layer-structured anisotropic metal chalcogenides: recent advances in synthesis, modulation, and applications. *Chemical Reviews* 123: 3329–3442.

3 Novoselov, K.S., Mishchenko, A., Carvalho, A., and Castro Neto, A.H. (2016). 2D materials and van der Waals heterostructures. *Science* 353 (6298): aac9439.

4 Polyushkin, D.K., Wachter, S., Mennel, L. et al. (2020). Analogue two-dimensional semiconductor electronics. *Nature Electronics* 3 (8): 486–491.

5 Chhowalla, M., Shin, H.S., Eda, G. et al. (2013). The chemistry of two-dimensional layered transition metal dichalcogenide nanosheets. *Nature Chemistry* 5 (4): 263–275.

6 Novoselov, K.S., Geim, A.K., Morozov, S.V. et al. (2004). Electric field effect in atomically thin carbon films. *Science* 306 (5696): 666–669.

7 Huang, Y., Sutter, E., Shi, N.N. et al. (2015). Reliable exfoliation of large-area high-quality flakes of graphene and other two-dimensional materials. *ACS Nano* 9 (11): 10612–10620.

8 Huang, Y., Pan, Y.-H., Yang, R. et al. (2020). Universal mechanical exfoliation of large-area 2D crystals. *Nature Communications* 11 (1): 2453.

9 Mak, K.F., Lee, C., Hone, J. et al. (2010). Atomically thin MoS_2: a new direct-gap semiconductor. *Physical Review Letters* 105 (13): 136805.

10 Radisavljevic, B., Radenovic, A., Brivio, J. et al. (2011). Single-layer MoS_2 transistors. *Nature Nanotechnology* 6 (3): 147–150.

11 Xin-Yu, H., Xu, H., Hui, C. et al. (2022). New progress and prospects of mechanical exfoliation technology of two-dimensional materials. *Acta Physica Sinica* 71 (10): 108201.

12 Guo, Q.B., Qi, X.-Z., Zhang, L.S. et al. (2023). Ultrathin quantum light source with van der Waals $NbOCl_2$ crystal. *Nature* 613 (7942): 53–59.

13 Deng, Y.J., Yu, Y.J., Song, Y.C. et al. (2018). Gate-tunable room-temperature ferromagnetism in two-dimensional Fe_3GeTe_2. *Nature* 563 (7729): 94–99.

14 Xu, X.L., Yang, S.Q., Wang, H. et al. (2022). Ferromagnetic-antiferromagnetic coexisting ground state and exchange bias effects in $MnBi_4Te_7$ and $MnBi_6Te_{10}$. *Nature Communications* 13 (1): 7646.

15 Wang, M.X., Zhang, J., Wang, Z.P. et al. (2019). Broadband CrOCl saturable absorber with a spectral region extension to 10.6 μm. *Advanced Optical Materials* 8 (2): 1901446.

16 Xi, X.X., Wang, Z.F., Zhao, W.W. et al. (2015). Ising pairing in superconducting $NbSe_2$ atomic layers. *Nature Physics* 12 (2): 139–143.

17 Zhang, B.Y., Xu, K., Yao, Q. et al. (2021). Hexagonal metal oxide monolayers derived from the metal–gas interface. *Nature Materials* 20 (8): 1073–1078.

18 Jiang, K., Ji, J.P., Gong, W.B. et al. (2022). Mechanical cleavage of non-van der Waals structures towards two-dimensional crystals. *Nature Synthesis* 2 (1): 58–66.

19 Pinilla, S., Coelho, J., Li, K. et al. (2022). Two-dimensional material inks. *Nature Reviews Materials* 7 (9): 717–735.

20 Coleman, J.N., Lotya, M., O'Neill, A. et al. (2011). Two-dimensional nanosheets produced by liquid exfoliation of layered materials. *Science* 331 (6017): 568–571.

21 Li, H.L., Jing, L., Liu, W.W. et al. (2018). Scalable production of few-layer boron sheets by liquid-phase exfoliation and their superior supercapacitive performance. *ACS Nano* 12 (2): 1262–1272.

22 Kaur, H. and Coleman, J.N. (2022). Liquid-phase exfoliation of nonlayered non-Van-Der-Waals crystals into nanoplatelets. *Advanced Materials* 34 (35): 2202164.

23 Cullen, P.L., Cox, K.M., Bin Subhan, M.K. et al. (2017). Ionic solutions of two-dimensional materials. *Nature Chemistry* 9 (3): 244–249.

24 Grayfer, E.D., Kozlova, M.N., and Fedorov, V.E. (2017). Colloidal 2D nanosheets of MoS_2 and other transition metal dichalcogenides through liquid-phase exfoliation. *Advances in Colloid and Interface Science* 245: 40–61.

25 Eda, G., Yamaguchi, H., Voiry, D. et al. (2011). Photoluminescence from chemically exfoliated MoS_2. *Nano Letters* 11 (12): 5111–5116.

26 Lam, D., Lebedev, D., Kuo, L. et al. (2022). Liquid-phase exfoliation of magnetically and optoelectronically active ruthenium trichloride nanosheets. *ACS Nano* 16 (7): 11315–11324.

27 Huo, C.X., Yan, Z., Song, X.F., and Zeng, H.B. (2015). 2D materials via liquid exfoliation: a review on fabrication and applications. *Scientific Bulletin* 60 (23): 1994–2008.

28 Ma, S., Li, G., Li, Z. et al. (2022). 2D Magnetic semiconductor Fe(3)GeTe(2) with few and single layers with a greatly enhanced intrinsic exchange bias by liquid-phase exfoliation. *ACS Nano* 16 (11): 19439–19450.

29 Yang, R., Mei, L., Zhang, Q. et al. (2022). High-yield production of mono- or few-layer transition metal dichalcogenide nanosheets by an electrochemical lithium ion intercalation-based exfoliation method. *Nature Protocols* 17 (2): 358–377.

30 Zeng, Z.Y., Yin, Z.Y., Huang, X. et al. (2011). Single-layer semiconducting nanosheets: high-yield preparation and device fabrication. *Angewandte Chemie, International Edition* 123 (47): 11289–11293.

31 Kappera, R., Voiry, D., Yalcin, S.E. et al. (2014). Phase-engineered low-resistance contacts for ultrathin MoS_2 transistors. *Nature Materials* 13 (12): 1128–1134.

32 Li, J., Song, P., Zhao, J.P. et al. (2021). Printable two-dimensional superconducting monolayers. *Nature Materials* 20 (2): 181–187.

33 Li, Y., Duerloo, K.A., Wauson, K., and Reed, E.J. (2016). Structural semiconductor-to-semimetal phase transition in two-dimensional materials induced by electrostatic gating. *Nature Communications* 7: 10671.

34 Wang, Y., Xiao, J., Zhu, H.Y. et al. (2017). Structural phase transition in monolayer $MoTe_2$ driven by electrostatic doping. *Nature* 550 (7677): 487–491.

35 Lin, Z.Y., Liu, Y., Halim, U. et al. (2018). Solution-processable 2D semiconductors for high-performance large-area electronics. *Nature* 562 (7726): 254–258.

36 Ciesielski, A. and Samori, P. (2016). Supramolecular approaches to graphene: from self-assembly to molecule-assisted liquid-phase exfoliation. *Advanced Materials* 28 (29): 1505371.

37 Chen, J.Y., Guo, Y.L., Wen, Y.G. et al. (2013). Two-stage metal-catalyst-free growth of high-quality polycrystalline graphene films on silicon nitride substrates. *Advanced Materials* 25 (7): 992–997.

38 Zheng, J.Y., Yan, X.X., Lu, Z.X. et al. (2017). High-mobility multilayered MoS_2 flakes with low contact resistance grown by chemical vapor deposition. *Advanced Materials* 29 (13): 1604540.

39 Zhou, J.D., Lin, J.H., Huang, X.W. et al. (2018). A library of atomically thin metal chalcogenides. *Nature* 556 (7701): 355–359.

40 Wang, Q., Li, N., Tang, J. et al. (2020). Wafer-scale highly oriented monolayer MoS_2 with large domain sizes. *Nano Letters* 20 (10): 7193–7199.

41 Sun, L.Z., Yuan, G.W., Gao, L.B. et al. (2021). Chemical vapour deposition. *Nature Reviews Methods Primers* 1 (1): 5.

42 Cai, Z.Y., Liu, B.L., Zou, X.L., and Cheng, H.-M. (2018). Chemical vapor deposition growth and applications of two-dimensional materials and their heterostructures. *Chemical Reviews* 118 (13): 6091–6133.

43 Wang, H., Chen, Y., Duchamp, M. et al. (2018). Large-area atomic layers of the charge-density-wave conductor $TiSe_2$. *Advanced Materials* 30 (8).

44 Hafeez, M., Gan, L., Li, H.Q. et al. (2016). Chemical vapor deposition synthesis of ultrathin hexagonal ReSe2 flakes for anisotropic raman property and optoelectronic application. *Advanced Materials* 28 (37): 8296–8301.

45 Wu, J.X., Tan, C.W., Tan, Z.J. et al. (2017). Controlled synthesis of high-mobility atomically thin bismuth oxyselenide crystals. *Nano Letters* 17 (5): 3021–3026.

46 Gao, T., Zhang, Q., Li, L. et al. (2018). 2D ternary chalcogenides. *Advanced Optical Materials* 6 (14): 1800058.

47 Tan, C.L. and Zhang, H. (2015). Epitaxial growth of hetero-nanostructures based on ultrathin two-dimensional nanosheets. *Journal of the American Chemical Society* 137 (38): 12162–12174.

48 van der Zande, A.M., Huang, P.Y., Chenet, D.A. et al. (2013). Grains and grain boundaries in highly crystalline monolayer molybdenum disulphide. *Nature Materials* 12 (6): 554–561.

49 Shi, Y.M., Li, H.N., and Li, L.-J. (2015). Recent advances in controlled synthesis of two-dimensional transition metal dichalcogenides via vapour deposition techniques. *Chemical Society Reviews* 44 (9): 2744–2756.

50 Gao, Y., Hong, Y.L., Yin, L.C. et al. (2017). Ultrafast growth of high-quality monolayer WSe_2 on Au. *Advanced Materials* 29 (29): 1700990.

51 Zhang, Z.W., Chen, P., Duan, X.D. et al. (2017). Robust epitaxial growth of two-dimensional heterostructures, multiheterostructures, and superlattices. *Science* 357 (6353): 788–792.

52 Liu, C., Xu, X.Z., Qiu, L. et al. (2019). Kinetic modulation of graphene growth by fluorine through spatially confined decomposition of metal fluorides. *Nature Chemistry* 11 (8): 730–736.

53 Kang, K., Xie, S.E., Huang, L.J. et al. (2015). High-mobility three-atom-thick semiconducting films with wafer-scale homogeneity. *Nature* 520 (7549): 656–660.

54 Chen, C., Chen, X.D., Wu, C.W. et al. (2022). Air-stable 2D Cr_5Te_8 nanosheets with thickness-tunable ferromagnetism. *Advanced Materials* 34 (2): 2107512.

55 Yan, C.Y., Gan, L., Zhou, X. et al. (2017). Space-confined chemical vapor deposition synthesis of ultrathin HfS2 flakes for optoelectronic application. *Advanced Functional Materials* 27 (39): 1702918.

56 Wang, Q., Shi, R., Zhao, Y.X. et al. (2021). Recent progress on kinetic control of chemical vapor deposition growth of high-quality wafer-scale transition metal dichalcogenides. *Nanoscale Advances* 3 (12): 3430–3440.

57 Dong, J.C., Zhang, L.N., Dai, X.Y., and Ding, F. (2020). The epitaxy of 2D materials growth. *Nature Communications* 11 (1): 5862.

58 Suenaga, K., Ji, H.G., Lin, Y.-C. et al. (2018). Surface-mediated aligned growth of monolayer MoS_2 and in-plane heterostructures with graphene on sapphire. *ACS Nano* 12 (10): 10032–10044.

59 Li, T.T., Guo, W., Ma, L. et al. (2021). Epitaxial growth of wafer-scale molybdenum disulfide semiconductor single crystals on sapphire. *Nature Nanotechnology* 16 (11): 1201–1207.

60 Yang, P.F., Liu, F.C., Li, X. et al. (2023). Highly reproducible epitaxial growth of wafer-scale single-crystal monolayer MoS_2 on sapphire. *Small Methods* 19: 2300165.

61 Ma, Z.P., Wang, S.Y., Deng, Q.X. et al. (2020). Epitaxial growth of rectangle shape MoS_2 with highly aligned orientation on twofold symmetry a-plane sapphire. *Small* 16 (16): 2000596.

62 Bian, R.J., Li, C.C., Liu, Q. et al. (2022). Recent progress in the synthesis of novel two-dimensional van der Waals materials. *National Science Review* 9 (5), nwab164.

63 Chen, T.A., Chuu, C.P., Tseng, C.C. et al. (2020). Wafer-scale single-crystal hexagonal boron nitride monolayers on Cu (111). *Nature* 579 (7798): 219–223.

64 Wang, L., Xu, X.Z., Zhang, L.N. et al. (2019). Epitaxial growth of a 100-square-centimetre single-crystal hexagonal boron nitride monolayer on copper. *Nature* 570 (7759): 91–95.

65 Xu, X.L., Pan, Y., Liu, S. et al. (2021). Seeded 2D epitaxy of large-area single-crystal films of the van der Waals semiconductor 2H $MoTe_2$. *Science* 372 (6538): 195–200.

66 Cheng, R., Jiang, S., Chen, Y. et al. (2014). Few-layer molybdenum disulfide transistors and circuits for high-speed flexible electronics. *Nature Communications* 5: 5143.

67 Li, S.L., Wakabayashi, K., Xu, Y. et al. (2013). Thickness-dependent interfacial coulomb scattering in atomically thin field-effect transistors. *Nano Letters* 13 (8): 3546–3552.

68 Liu, Y.C. and Gu, F.X. (2021). A wafer-scale synthesis of monolayer MoS_2 and their field-effect transistors toward practical applications. *Nanoscale Advances* 3 (8): 2117–2138.

69 Kim, S., Konar, A., Hwang, W.S. et al. (2012). High-mobility and low-power thin-film transistors based on multilayer MoS_2 crystals. *Nature Communications* 3: 1011.

70 Yan, J., Xia, J., Wang, X. et al. (2015). Stacking-dependent interlayer coupling in trilayer MoS_2 with broken inversion symmetry. *Nano Letters* 15 (12): 8155–8161.

71 Zhang, X.M., Nan, H.Y., Xiao, S.Q. et al. (2019). Transition metal dichalcogenides bilayer single crystals by reverse-flow chemical vapor epitaxy. *Nature Communications* 10 (1): 598.

72 Han, A., Aljarb, A., Liu, S. et al. (2019). Growth of 2H stacked WSe_2 bilayers on sapphire. *Nanoscale Horizons* 4 (6): 1434–1442.

73 Li, J.W., Wang, S.P., Li, L. et al. (2022). Chemical vapor deposition of 4 inch wafer-scale monolayer $MoSe_2$. *Small Science* 2 (11): 2200062.

74 Wang, Q.Q., Tang, J., Li, X.M. et al. (2022). Layer-by-layer epitaxy of multi-layer MoS_2 wafers. *National Science Review* 9 (6), nwac077.

75 Li, X.F., Zhang, Z.F., Gao, T.T. et al. (2022). Van der Waals epitaxial trilayer MoS_2 crystals for high-speed electronics. *Advanced Functional Materials* 32 (46): 2208091.

76 Liu, L., Li, T.T., Ma, L. et al. (2022). Uniform nucleation and epitaxy of bilayer molybdenum disulfide on sapphire. *Nature* 605 (7908): 69–75.

77 Ma, W., Chen, M.L., Yin, L.C. et al. (2019). Interlayer epitaxy of wafer-scale high-quality uniform AB-stacked bilayer graphene films on liquid Pt_3Si/solid Pt. *Nature Communications* 10 (1): 2809.

78 Zhang, Z.B., Ding, M.C., Cheng, T. et al. (2022). Continuous epitaxy of single-crystal graphite films by isothermal carbon diffusion through nickel. *Nature Nanotechnology* 17 (12): 1258–1264.

79 Ma, K.Y., Zhang, L., Jin, S. et al. (2022). Epitaxial single-crystal hexagonal boron nitride multilayers on Ni (111). *Nature* 606 (7912): 88–93.

80 Li, W.B., Qian, X.F., and Li, J. (2021). Phase transitions in 2D materials. *Nature Reviews Materials* 6 (9): 829–846.

81 Park, J.C., Yun, S.J., Kim, H. et al. (2015). Phase-engineered synthesis of centimeter-scale 1T′- and 2H-molybdenum ditelluride thin films. *ACS Nano* 9 (6): 6548–6554.

82 Qian, X.f., Liu, J.w., Fu, L., and Li, J. (2014). Quantum spin Hall effect in two-dimensional transition metal dichalcogenides. *Science* 346 (6215): 1344–1347.

83 Keum, D.H., Cho, S., Kim, J.H. et al. (2015). Bandgap opening in few-layered monoclinic $MoTe_2$. *Nature Physics* 11 (6): 482–486.

84 Kang, L.X., Ye, C., Zhao, X.X. et al. (2020). Phase-controllable growth of ultra-thin 2D magnetic FeTe crystals. *Nature Communications* 11 (1): 3729.

85 Zhang, S.C., Wu, Y., Gao, F. et al. (2022). Field effect transistor sensors based on in-plane 1T′/2H/1T′ $MoTe_2$ heterophases with superior sensitivity and output signals. *Advanced Functional Materials* 32 (41): 2205299.

86 Tang, L., Tan, J.Y., Nong, H.Y. et al. (2020). Chemical vapor deposition growth of two-dimensional compound materials: controllability, material quality, and growth mechanism. *Accounts of Materials Research* 2 (1): 36–47.

87 Liu, L., Wu, J.X., Wu, L.Y. et al. (2018). Phase-selective synthesis of 1T' MoS_2 monolayers and heterophase bilayers. *Nature Materials* 17 (12): 1108–1114.

88 Deng, Q.X., Li, X.B., Si, H.Y. et al. (2020). Strong band bowing effects and distinctive optoelectronic properties of 2H and 1T′ phase-tunable $MoxRe_1–xS_2$ Alloys. *Advanced Functional Materials* 30 (34): 2003264.

89 Han, W., Zheng, X.D., Yang, K. et al. (2023). Phase-controllable large-area two-dimensional In_2Se_3 and ferroelectric heterophase junction. *Nature Nanotechnology* 18 (1): 55–63.